Available online at www.sciencedirect.com
SCIENCE DIRECT®
Journal of Solid State Chemistry 177 (2004) 4269–4281
JOURNAL OF SOLID STATE CHEMISTRY
www.elsevier.com/locate/jssc

New alkaline earth-zirconium oxalates $M_2Zr(C_2O_4)_4 \cdot nH_2O$ (M = Ba, Sr, Ca) synthesis, crystal structure and thermal behavior

B. Chapelet-Arab[a,b], G. Nowogrocki[a], F. Abraham[a,*], S. Grandjean[b]

[a] *Laboratoire de Cristallochimie et Physicochimie du Solide, Universite des Sciences et Technologies de Lille, UMR CNRS 8012, ENSCL-USTL, B.P. 108, 59652 Villeneuve d'Ascq Cedex, France*

[b] *Laboratoire de Chimie des Actinides, CEA VALRHO/DRCP/SCPS, Bât 399 BP 17171 30208 Bagnols sur Ceze Cedex, France*

Received 6 April 2004; received in revised form 24 June 2004; accepted 26 June 2004

Abstract

Three new alkaline earth-zirconium oxalates $M_2Zr(C_2O_4)_4 \cdot nH_2O$ have been synthesized by precipitation methods for M = Ba, Sr, Ca. For each compound the crystal structure was determined from single crystals obtained by controlled diffusion of M^{2+} and Zr^{4+} ions through silica gel containing oxalic acid. $Ba_2Zr(C_2O_4)_4 \cdot 7H_2O$, monoclinic, space group $C2/c$, $a = 9.830(2)$, $b = 29.019(6)$, $c = 9.178(2)$ Å, $\beta = 122.248(4)°$, $V = 2214.2(8)$ Å^3, $Z = 4$, $R = 0.0427$; $Sr_2Zr(C_2O_4)_4 \cdot 11H_2O$, tetragonal, space group $I4_1/acd$, $a = 16.139(4)$, $c = 18.247(6)$ Å, $V = 4753(2)$ Å^3, $Z = 8$, $R = 0.0403$; $Ca_2Zr(C_2O_4)_4 \cdot 5H_2O$, orthorhombic, space group $Pna2_1$, $a = 8.4181(5)$, $b = 15.8885(8)$, $c = 15.8885(8)$ Å, $V = 2125(2)$ Å^3, $Z = 4$, $R = 0.0622$. The structures of the three compounds consist of chains of edge-shared $MO_6(H_2O)_x$ ($x = 2$ or 3) polyhedra connected to ZrO_8 polyhedra through oxalate groups. Depending on the arrangement of chains, the ZrO_8 polyhedron geometry (dodecahedron or square antiprism) and the connectivity, two types of three-dimensional frameworks are obtained. For the smallest M^{2+} cations (Sr^{2+}, Ca^{2+}), large tunnels are obtained, running down the c direction of the unit cell, which can accommodate zeolitic water molecules. For the largest Ba^{2+} cation, the second framework is formed and is closely related to that of $Pb_2Zr(C_2O_4)_4 \cdot nH_2O$. The decomposition at 800°C into strontium carbonate, barium carbonate or calcium oxide and $MZrO_3$ (M = Sr, Ba, Ca) perovskite is reported from thermal analyses studies and high temperature X-ray powder diffraction.

Keywords: Zirconium oxalate; Alkaline earth oxalate; Crystal structure refinement; Thermal behavior

1. Introduction

A lot of publications has been devoted in recent years to the preparation of oxalates of metallic ions or mixture of metallic ions. The principal aim of these studies was the synthesis of oxides or mixed oxides by decomposition of oxalate precursors at rather low temperature: a well-known example is the production of $BaTiO_3$ from the barium titanium oxalate [1].

In these former studies, the oxalate ion $C_2O_4^{2-}$ was found to show a large variety in structural characteristics. It can act as monodentate, bidentate, tridentate or tetradentate donor ligand and can form with metal centers chains, layers or three-dimensional networks. Combined with the presence of water molecules directly linked to the metal ions or weakly bonded to the framework, this leads to a very large variety of structural architectures in one-, two- or three dimensions.

Among the metallic ions studied, Zr^{4+} has attracted a great deal of interest because it has a rather simple coordination geometry: indeed, with oxy-ligands, it is very frequently eight-fold coordinated and has a square antiprism [2–4] or a dodecahedral arrangement [5–7].

If zirconium oxalate has been proposed for the synthesis of pure and stabilized zirconia [8], surprisingly enough, double oxalates of zirconium and alkaline earth

*Corresponding author. Fax: +33-3-20-43-68-14.
E-mail address: francis.abraham@ensc-lille.fr (F. Abraham).

0022-4596/$ - see front matter © 2004 Elsevier Inc. All rights reserved.
doi:10.1016/j.jssc.2004.06.053

metals were not characterized, the only studies concerning the thermal decomposition of zirconyl oxalates of alkaline earth metals $MZrO(C_2O_4)_2 \cdot nH_2O$ (M = Ba, Sr, Ca) [9–16] and calcium zirconium oxalate $CaZr(C_2O_4)_3 \cdot 1H_2O$ [17] leading to the corresponding perovskite $MZrO_3$. Actually, the formula of the mixed oxalates of M and Zr was not unambiguously established, thus we have undertaken the single-crystal growth and the crystal structure determination of these compounds.

In fact a new series of mixed oxalates $M_2Zr(C_2O_4)_4 \cdot nH_2O$ ($M = Ba^{2+}$, Sr^{2+}, Ca^{2+}), which cannot lead by thermal decomposition to pure perovskite, was obtained and the present paper deals with the synthesis, the crystal structure determination and the thermal behavior of this new series and focuses on the main differences and similarities between the members of this family.

2. Experimental

2.1. Single crystal and powder synthesis

The growth of single crystals of double oxalates $M_2Zr(C_2O_4)_4 \cdot nH_2O$ ($M = Ba^{2+}$, Sr^{2+}, Ca^{2+}), suitable for X-ray diffraction study, is accomplished by the controlled diffusion of the divalent cation M^{2+} and the zirconium ions through silica gel impregnated with oxalic acid [18]. The silica gel is prepared by pouring sodium metasilicate solution into a mixture of 1 M oxalic acid and 3 M nitric acid so as to get a pH between 3.5 and 4. Nitric acid is used to acidify the medium and oxalic acid as a source of anions. The resulting solution is then allowed to set in tubes of internal diameter 15 mm. Then, when the aqueous solution of the divalent cation M^{2+} nitrate (0.25 M, 10 mL) and zirconium oxynitrate (0.25 M, 5 mL), acidified by 3 M nitric acid (7.5 mL) is slowly added on the set gel, crystals of $M_2Zr(C_2O_4)_4 \cdot nH_2O$ can form slowly inside the gel.

Transparent stacked platelet single crystals of $Ba_2Zr(C_2O_4)_4 \cdot 7H_2O$ are obtained, whereas with Ca^{2+} and Sr^{2+}, bipyramidal transparent crystals of average size 100 μm were prepared.

In order to study the thermal decomposition of these new mixed oxalate compounds, powders corresponding to the crystals analyzed by X-ray diffraction, were precipitated. These precipitates were formed under constant stirring, from the titration of the mixture of nitric acid and oxalic acid by an aqueous solution of the divalent cation M^{2+} and zirconium oxynitrate acidified by nitric acid. Oxalic acid was introduced in excess to ensure the complete precipitation. The resulting powders were filtered off, dried at room temperature and characterized by X-ray diffraction. These precipitates were found to be very sensitive to the storage conditions, such as the water-vapor pressure in ambient atmosphere. Indeed, the compounds can lose spontaneously one or several water molecules and so all of these powders were stored in a closed recipient in presence of water in order to ensure a nearly constant water-vapor pressure above the precipitate.

2.2. Collection of X-ray powder diffraction data

X-ray powder diffraction data were obtained with a Huber Imaging Plate Guinier Camera G670 diffractometer using monochromated Cu$K\alpha_1$ radiation (λ = 1.5406 Å) isolated by a germanium monochromator.

High Temperature X-ray diffraction (HTXRD) experiments were performed under dynamic air, saturated by water-vapor, with a SIEMENS D5000 powder diffractometer (graphite monochromator and Cu$K\bar{\alpha}$ radiation), equipped with a HTK 1200 Anton Paar device and a scintillation detector. The sample was deposited on an alumina holder. Several diagrams were recorded between ambient temperature and 800 °C, in the 10–60° 2θ domain, with a step of 0.02° (2θ), a counting time of 5 s (i.e. a diagram was recorded in about 4 h), and a heating rate of 0.08 °C s^{-1}.

2.3. Single-crystal data collection

The single-crystal diffraction intensities for each compound were measured on an AXS BRUKER SMART CCD-1 K diffractometer system equipped with a fine-focus Mo-target X-ray tube (λ = 0.71073 Å) operated at 2000 watts power. The detector was placed at a distance of 5.41 cm from the crystal. The intensities were obtained under the conditions given in Table 1 and extracted from the collected frames using the program SaintPlus 6.02 [19]. The structure resolutions and refinements were performed with the JANA2000 software package [20]. The lattice parameters were refined from the complete data set and an absorption correction, empirical for M = Ba and based on the faces indices for M = Sr, Ca, was performed [21]. The heavy atoms were located using the direct methods, while the remaining atoms were found from successive Fourier map analyses. The hydrogen atoms of water molecules could not be located because of the important thermal agitation of water molecules. The atomic positions for all atoms and the anisotropic displacement parameters were included in the last cycles of refinement.

2.4. Thermal analysis

Thermogravimetric analyses (TG) were carried out with a SETARAM 92 thermal analysis system with a platinum crucible up to 800 °C, under air and with a scan rate of 1 °C min^{-1}.

Table 1
Crystal data and structure refinement parameters for $Ba_2Zr(C_2O_4)_4 \cdot 7H_2O$, $Sr_2Zr(C_2O_4)_4 \cdot 11H_2O$ and $Ca_2Zr(C_2O_4)_4 \cdot 5H_2O$

Empirical formula	$Ba_2ZrC_8O_{23}H_{14}$	$Sr_2ZrC_8O_{27}H_{22}$	$Ca_2ZrC_8O_{21}H_{10}$
Formula weight g mol^{-1}	843.9	816.5	613.4
Crystal system	Monoclinic	Tetragonal	Othorhombic
Space group	$C2/c$	$I4_1/acd$	$Pna2_1$
Crystal size mm	$0.5 \times 0.1 \times 0.04$	$0.6 \times 0.45 \times 0.3$	$0.6 \times 0.6 \times 0.5$
a (Å)	9.830(2)	16.139(4)	8.4181(5)
b (Å)	29.019(6)	16.139(4)	15.8885(8)
c (Å)	9.178(2)	18.247(6)	15.8885(8)
α	90	90	90
β	122.248(4)	90	90
γ	90	90	90
Volume (Å^3)	2214.2(8)	4753(2)	2125(2)
Z	4	8	4
ρ_{calc} (Mg/m^3)	2.53	2.28	1.92
Absorption coefficient (mm^{-1})	4.084	5.023	1.047
Absorption correction	Empirical	Gaussian faces-indexed	Gaussian faces-indexed
Max and min transmission		0.420 and 0.199	0.790 and 0.640
$F(000)$	1536	3040	1184
Temperature (K)	293(2)	293(2)	293(2)
Wavelength (Å)	0.71073	0.71073	0.71073
θ range (deg)	1.40–30.99	2.52–28.33	2.56–28.20
Index ranges	$-13 \leqslant h \leqslant 13$	$-18 \leqslant h \leqslant 21$	$-10 \leqslant h \leqslant 10$
	$-41 \leqslant k \leqslant 41$	$-21 \leqslant k \leqslant 21$	$-2 \leqslant k \leqslant 19$
	$-13 \leqslant l \leqslant 12$	$-23 \leqslant l \leqslant 23$	$-20 \leqslant l \leqslant 21$
Reflections collected	10,892	13,340	12,352
Independent reflections	3229	1426	7399
	$[R_{int} = 0.0535]$	$[R_{int} = 0.0309]$	$[R_{int} = 0.0281]$
Completeness = 95%	$\theta = 30.33^\circ$	$\theta = 28.33^\circ$	$\theta = 27.58^\circ$
Refinement method	Full-matrix	Full-matrix	Full-matrix
	Least-squares on F	Least-squares on F	Least-squares on F
Weighting scheme	Sigma	Sigma	Unit
Data/restraints/parameters	3229/0/174	1426/0/122	7399/0/144
Final R indices $[I > 3\sigma(I)]$	$R = 0.0427$,	$R = 0.0403$,	$R = 0.0622$,
	$wR = 0.0430$	$wR = 0.0458$	$wR = 0.0586$
R indices (all data)	$R_{all} = 0.0695$,	$R_{all} = 0.0544$,	$R_{all} = 0.0942$,
	$wR_{all} = 0.0447$	$wR_{all} = 0.0464$	$wR_{all} = 0.0735$
Largest diff. peak and hole e Å^{-3}	3.31 and −1.91	1.34 and −0.650	1.30 and −0.94

3. Results and discussion

3.1. $Ba_2Zr(C_2O_4)_4 \cdot 7H_2O$

3.1.1. Structure description

The crystal structure of $Ba_2Zr(C_2O_4)_4 \cdot 7H_2O$ was solved with the monoclinic symmetry in the space group $C2/c$. The refined atomic positions are given in Table 2 and selected bond distances and angles are reported in Table 3.

The three-dimensional crystal structure of $Ba_2Zr(C_2O_4)_4 \cdot 7H_2O$ is built from zirconium and barium polyhedra linked by oxalate groups. In each asymmetric unit, the two crystallographically independent barium (II) atoms are nine-fold coordinated by six oxygen atoms from two bidentate and two monodentate oxalate groups (Ba–O distances range from 2.80 to 2.96 Å for Ba(1) and from 2.76 to 2.85 Å for Ba(2)) and by three water molecules (Fig. 1). Around the barium atom Ba(2), the calculated positions of oxygen atoms O(w11), O(w12) and O(w13) are too close, so a partial occupancy (Table 2) has been introduced which leads to the presence of three water molecules in the environment of Ba(2) (distances range from 2.74 to 2.95 Å). The zirconium(IV) is eight-fold coordinated by oxygen atoms from four bidentate oxalate ligands and located between 2.16 and 2.21 Å from the zirconium atom. The 16th, 17th and 18th lowest O–Zr–O′ angles are 84.68°, 98.6° and 116.6°, respectively, then using the criteria developed by HAIGH [22] to distinguish the types of structures in eight-coordinated complexes, the zirconium polyhedra ZrO_8 could be classified as square antiprism distorted towards biccaped trigonal prism or hendecahedron (Fig. 1).

Two of the four oxalate units that link Ba(1) atoms are shared between two neighboring Ba(1) atoms via O(6) oxygen atoms that gives rise to one-dimensional chains of edge-shared $Ba(1)O_9$ polyhedra (Fig. 2). These chains running down the [101] direction are arranged side by side in the (010) plane at $y \approx 0.25$ and 0.75. In

Table 2
Atomic coordinates and equivalent isotropic displacement parameters ($Å^2$) for $Ba_2Zr(C_2O_4)_4 \cdot 7H_2O$

Atom	Site	Occup	x	y	z	U_{eq}
Ba(1)	4*e*	1	0	0.2215(1)	3/4	0.024(1)
Ba(2)	4*e*	1	1/2	0.0205(1)	1/4	0.032(1)
Zr(3)	4*e*	1	0	0.1347(1)	1/4	0.021(1)
C(1)	8*f*	1	0.2630(7)	0.0628(2)	0.4178(8)	0.032(1)
C(2)	8*f*	1	0.2218(8)	0.0727(2)	0.5532(8)	0.036(2)
O(1)	8*f*	1	0.1814(5)	0.0858(2)	0.2800(5)	0.033(1)
O(2)	8*f*	1	0.3688(6)	0.0347(2)	0.4478(6)	0.039(1)
O(3)	8*f*	1	0.2972(8)	0.0536(2)	0.6933(7)	0.075(2)
O(4)	8*f*	1	0.1047(5)	0.1003(2)	0.5027(5)	0.030(1)
C(3)	8*f*	1	0.2085(7)	0.1933(2)	0.1722(7)	0.024(1)
C(4)	8*f*	1	0.2970(7)	0.1954(2)	0.3694(7)	0.027(1)
O(5)	8*f*	1	0.0694(5)	0.1739(1)	0.0993(5)	0.026(1)
O(6)	8*f*	1	0.2666(5)	0.2093(2)	0.0954(5)	0.033(1)
O(7)	8*f*	1	0.2204(5)	0.1748(1)	0.4274(5)	0.029(1)
O(8)	8*f*	1	0.4259(5)	0.2151(2)	0.4515(5)	0.038(1)
O(w9)	4*e*	1	0	0.1255(3)	3/4	0.063(2)
O(w10)	8*f*	1	0.2750(6)	0.1937(3)	0.7574(6)	0.068(2)
O(w11)	8*f*	1/2	0.3970(20)	0.1040(6)	0.0390(20)	0.088(5)
O(w12)	8*f*	1/2	0.2890(20)	0.0763(7)	−0.0170(20)	0.114(7))
O(w13)	8*f*	1/2	0.1508(15)	0.0306(6)	0.0056(18)	0.083(4)
O(w14)	8*f*	1/2	0.0079(17)	0.0141(6)	−0.1755(17)	0.089(4)

U_{eq} is defined as one third of the trace of the orthogonalized U_{ij} tensor.

Table 3
Most important bond lengths (Å) and angles (deg) for $Ba_2Zr(C_2O_4)_4 \cdot 7H_2O$

Within the $Ba1O_9$ polyhedra		Within the $Ba2O_9$ polyhedra	
Ba(1)–O(6)^{II}	2.798(4)	Ba(2)–O(2)^{VI}	2.762(4)
Ba(1)–O(6)^{III}	2.798(4)	Ba(2)–O(2)	2.762(4)
Ba(1)–O(6)^{IV}	2.859(4)	Ba(2)–O(3)^{VII}	2.785(5)
Ba(1)–O(6)^{V}	2.859(4)	Ba(2)–O(3)^{VIII}	2.785(5)
Ba(1)–O(8)^{II}	2.961(5)	Ba(2)–O(2)^{VII}	2.846(4)
Ba(1)–O(8)^{III}	2.961(5)	Ba(2)–O(2)^{VIII}	2.846(4)
Ba(1)–O(w9)	2.786(8)	Ba(2)–O(w11)^{VI}	2.928(13)
Ba(1)–O(w10)^{I}	2.787(5)	Ba(2)–O(w11)	2.928(13)
Ba(1)–O(w10)	2.787(5)	Ba(2)–O(w12)^{VI}	2.740(17)
		Ba(2)–O(w12)	2.740(16)
		Ba(2)–O(w13)^{VI}	2.947(13)
		Ba(2)–O(w13)	2.947(13)
Within the ZrO_8 polyhedra			
Zr(3)–O(5)	2.163(4)		
Zr(3)–O(5)^{IV}	2.163(4)		
Zr(3)–O(1)^{IV}	2.179(4)		
Zr(3)–O(1)	2.179(4)		
Zr(3)–O(4)^{IV}	2.211(4)		
Zr(3)–O(4)	2.211(4)		
Zr(3)–O(7)	2.221(4)		
Zr(3)–O(7)^{IV}	2.221(4)		
Within the oxalate groups			
C(1)–O(2)	1.232(7)	O(2)–C(1)–O(1)	125.5(6)
C(1)–O(1)	1.267(7)	O(2)–C(1)–C(2)	120.1(6)
C(1)–C(2)	1.526(9)	O(1)–C(1)–C(2)	114.3(5)
C(2)–O(3)	1.222(8)	O(3)–C(2)–O(4)	126.4(6)
C(2)–O(4)	1.269(7)	O(3)–C(2)–C(1)	119.7(6)
		O(4)–C(2)–C(1)	113.9(5)
C(3)–O(6)	1.212(7)	O(6)–C(3)–O(5)	124.4(5)
C(3)–O(5)	1.287(7)	O(6)–C(3)–C(4)	121.6(5)
C(3)–C(4)	1.535(7)	O(5)–C(3)–C(4)	114.0(5)
C(4)–O(8)	1.218(7)	O(8)–C(4)–O(7)	127.7(5)
C(4)–O(7)	1.279(7)	O(8)–C(4)–C(3)	119.7(5)
		O(7)–C(4)–C(3)	112.5(5)

Symmetry transformations used to generate equivalent atoms: I, x, y, $-z+3/2$; II, $-x+1/2$, $-y+1/2$, $-z+1$; III, $x-1/2$, $-y+1/2$, $z+1/2$; IV, $-x$, y, $-z+1/2$; V, x,y,$z+1$; VI, $-x+1$, y, $-z+1/2$; VII, x, $-y$, $z-1/2$; VIII, $-x+1$, $-y$, $-z+1$.

the same way $Ba(2)O_9$ polyhedra are linked together by O(2)–O(2) edges to form one-dimensional chains parallel to the [001] direction and arranged in the (010) plane at at $y \approx 0.0$ and 0.5. The four oxalate units that link Zr atoms have the normal bidentate connectivity, so the ZrO_8 polyhedra are isolated one from another, they are also arranged in (010) planes at $y \approx 0.125$, 0.375, 0.625 and 0.875 and connected to the $Ba(1)O_9$ and $Ba(2)O_9$ polyhedra via the bis-bidentate oxalate moieties. Thus the three-dimensional framework results from the stacking along [010] of layered arrangements connected via oxalate groups in the succession –Ba(1)–Zr–Ba(2)–Zr–. This structural arrangement is very similar to that found by Boudaren et al. [2] for the lead zirconium oxalate hydrate $Pb_2Zr(C_2O_4)_4 \cdot nH_2O$ ($3 < n < 9$).

Within the two crystallographically independent oxalate ligands of the structure, the various bond lengths and angles (distances C–O range from 1.21 to 1.29 Å and C–C from 1.52 to 1.54 Å, average angle O–C–O is 126(1)° and O–C–C is 117(1)°) are in good agreement with the mean values reported by Hahn for oxalate compounds [23]: C–O = 1.24 Å, C–C = 1.55 Å, O–C–O = 125°, O–C–C = 117°.

In this structure, there is only one "free or zeolitic" water molecule per asymmetric unit half-occupying a general 8*g* site (O(w14)–O(w14) = 1.29 Å) which is localized in the tunnels running down [010] in the space which separates two Ba(2) oxalate chains and ZrO_8 polyhedra (Fig. 2).

3.1.2. Thermal decomposition

The thermal behavior of the mixed oxalate compound was studied by TG measurements and by HTXRD from room temperature to 800 °C (Figs. 3 and 4). The water content (7 water molecules) and then the chemical formula ($Ba_2Zr(C_2O_4)_4 \cdot 7H_2O$) have been deduced from the TG measurements (15.1% weigh loss) and agree with the formula found from crystal structure determination. This water content is very difficult to determine precisely because of the spontaneously loss at room temperature of some water molecules, so the powder must be kept with a constant water-vapor pressure in order to be sure of the powder water composition. For the HTXRD analysis, the airflow must be saturated by water to prevent a too early dehydration phenomenon, which leads to the modification of the crystallographic data of the product. Indeed, between the HTXRD

diagram at room temperature and the diagram at 100 °C, the loss of some water molecules caused the displacement of the main crystallographic reflections.

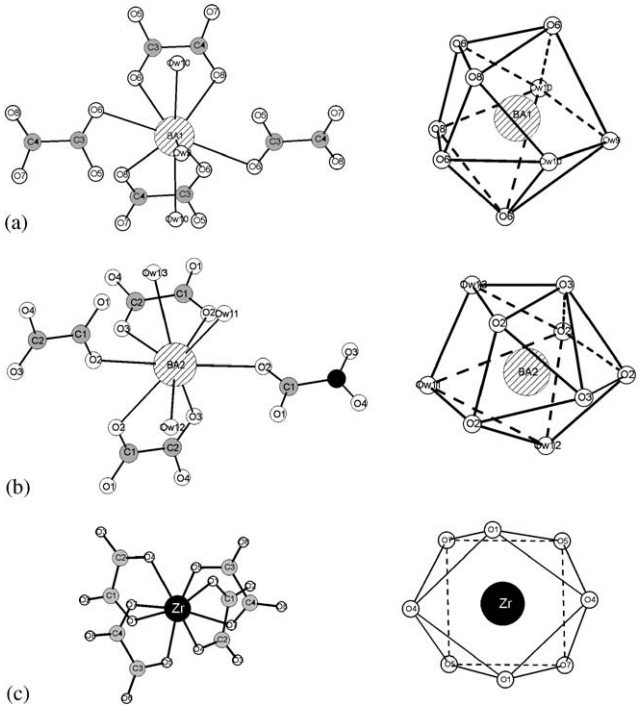

Fig. 1. Coordination spheres for (a) Ba(1), (b) Ba(2) and (c) Zr in $Ba_2Zr(C_2O_4)_4 \cdot 7H_2O$.

The joint investigations of the results of TG measurements and HTXRD analysis allow to identify the decomposition stages of this mixed barium-zirconium oxalate compound. First, in the interval from room temperature to 200 °C, endothermic reactions releasing 2 and 5 water molecules follow each other closely (total weight loss 15.1% against expected value 15.0%). This results in the formation of the anhydrous product ($Ba_2Zr(C_2O_4)_4$), which is totally amorphous and has a large stability domain (between 200 and 300 °C). The third stage occurs in the interval

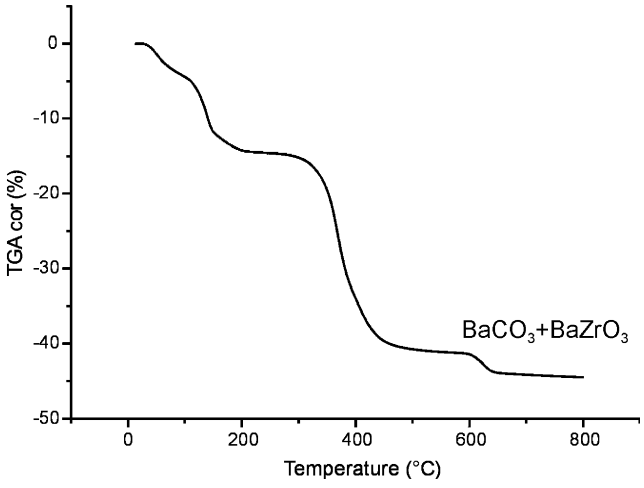

Fig. 3. TG curve for $Ba_2Zr(C_2O_4)_4 \cdot 7H_2O$ under flowing air (1 °C min^{-1}) with identified crystalline compounds.

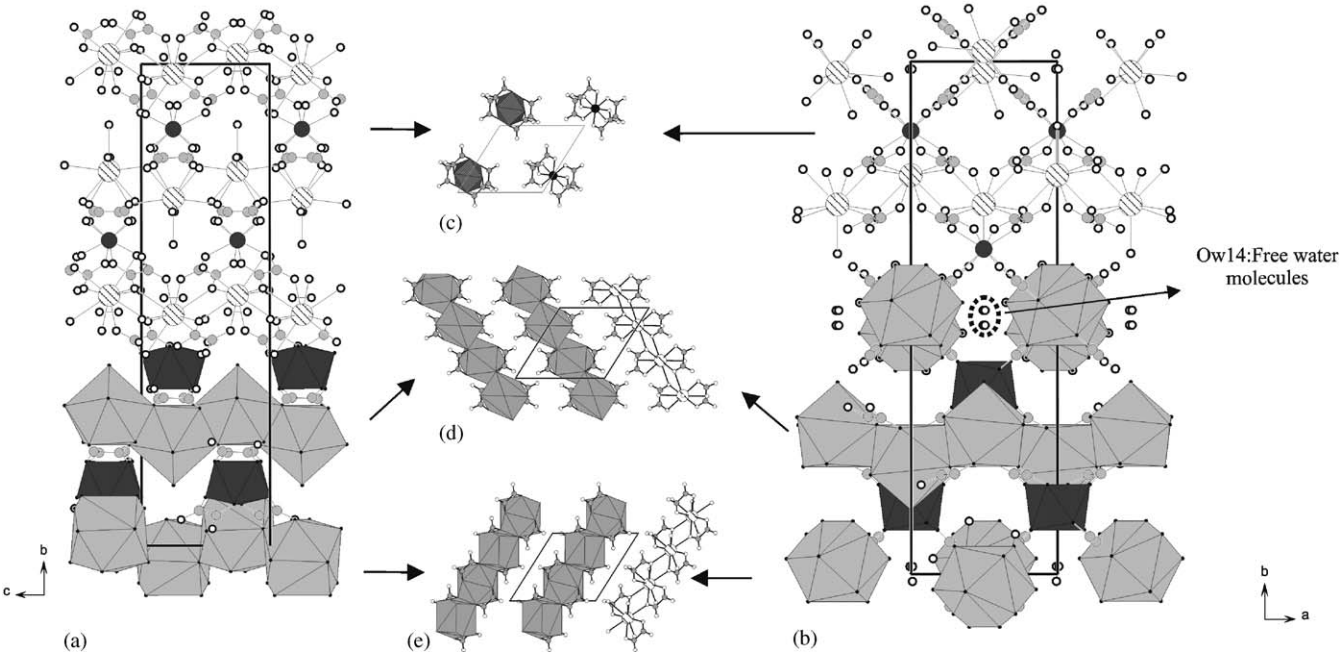

Fig. 2. Projections of the structure of $Ba_2Zr(C_2O_4)_4 \cdot 7H_2O$ down the *a*-axis (a) and the *b*-axis (b). The arrangement of the chains of edge-shared Ba(1) and Ba(2) polyhedra in (010) planes at $y \sim 0$ and 0.5 and at $y \sim 0.25$ and 0.75 are shown on (d) and (e), respectively. The ZrO_8 polyhedra are arranged in planes (010) at $y \sim \pm 0.125$ and ± 0.375 (c). Large hatching circle, Ba; medium black circle , Zr; small light-gray circle, C; small white circle, O.

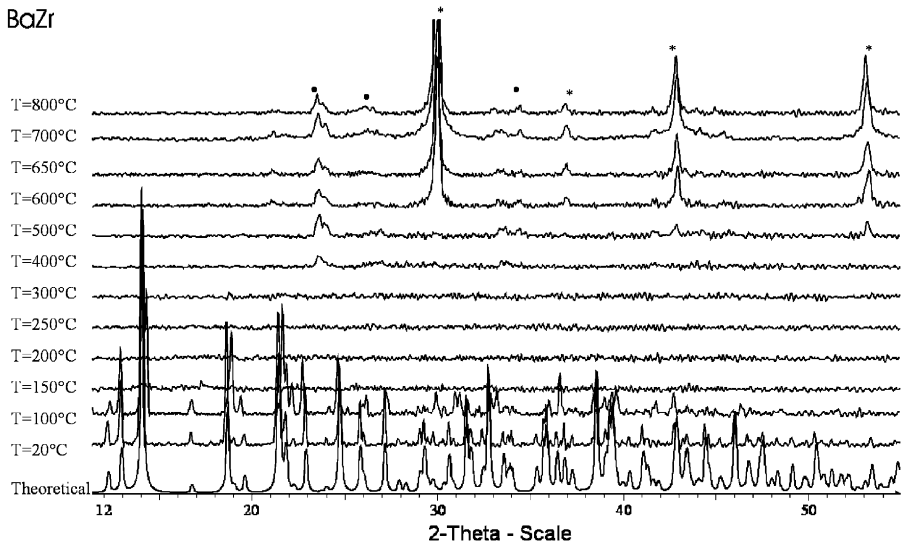

Fig. 4. HTXRD plot for for $Ba_2Zr(C_2O_4)_4 \cdot 7H_2O$ under water saturated flowing air; ●, diffraction lines from $BaCO_3$; ∗, diffraction lines from $BaZrO_3$. The X-ray diagram noted "theoretical" is calculated from the single-crystal data by the software POWDERCELL.

300–500 °C and the resulting powder is black. The X-ray diffraction analysis of the TG residue at 600 °C and the HTXRD diagram at 600 °C show that this black powder contains a mixture of barium carbonate ($BaCO_3$) and barium-zirconium oxide ($BaZrO_3$). The color of the powder implies the presence of carbon C and the weight loss determined by TG measurement (41.2%) does not agree with the formation of a mix containing only $BaCO_3$ and $BaZrO_3$ (calculated weigh loss: 43.9%). Then, this intermediate compound must be a mixture of barium carbonate, barium zirconium oxide, carbon C and perhaps an amorphous barium zirconium oxycarbonate which cannot be precisely identified. Reddy et al. [9] in their work on the decomposition of barium zirconyl oxalate, have mentioned the presence of carbon in the residue below 650 °C and the formation of the oxycarbonate $Ba_2Zr_2O_5CO_3(CO)$.

Between 550 and 650 °C, carbon monoxide is released due to the oxidation of carbon. The final product is a white powder (all the carbon has disappeared) and must be a mixture of crystallized $BaZrO_3$ and $BaCO_3$. The following residue composition $BaCO_3 + BaZrO_3$ which calculated value of the total weigh loss is 43.9%, agrees with TG measurements (weigh loss 44.8%). The presence in the residue of barium carbonate $BaCO_3$ and barium zirconium oxide $BaZrO_3$ have been confirmed by the HTXRD analysis.

3.2. $Sr_2Zr(C_2O_4)_4 \cdot 11H_2O$

3.2.1. Structure description

The structure resolution was not straightforward. If the crystal chosen is too small (<100 μm), the cell found by the indexing software is tetragonal with $a = 11.41$ Å, $c = 9.12$ Å. In this cell, close to the one proposed by Jeanneau et al. [6] for $Cd_2Zr(C_2O_4)_4 \cdot nH_2O$, no satisfactory space group could be proposed unambiguously. When a sufficient big crystal (>150 μm) was used, existence of weak spots led to multiply the previous cell parameters ($a \times \sqrt{2}$, $c \times 2$) and get a good solution. Moreover, the choice of the single crystal analyzed by X-ray diffraction is difficult because these crystals are very sensitive to dehydration outside their growth medium and this phenomenon leads to partial lost of the crystallinity of the compound during the X-ray analysis. So, this type of crystal must be stored and studied in a glass capillary in presence of water.

The structure was then solved in a tetragonal symmetry in space group $I4_1/acd$ with lattice parameters $a = 16.139(4)$ Å and $c = 18.247(6)$ Å (Table 1). The isotropic displacement parameters of the water molecules Ow(1) and Ow(2) were high so the crystallographic positions of these molecules have been split into two close sites (Ow(1A) and Ow(1B) for Ow(1); Ow(2A) and Ow(2B) for Ow(2)). These different positions of the water molecules are too close each other (distance Ow(1A)–Ow(1B) 0.86 Å, Ow(2A)–Ow(2B) 1.24 Å), so the occupancy rate of each site is partial. Moreover, whereas the oxygen atom Ow(2) lied in a special position, Ow(2A) and Ow(2B) lie on general positions, the total occupancy of these two sites has to be fixed to 0.5 (0.41 for Ow(2A) position and 0.09 for Ow(2B) position, Table 4) to keep the right number of water molecules. The distance between oxygen atoms Ow(4A) and Ow(4B) is too short (distance Ow(4A)–Ow(4B) = 0.82 Å), so they can not be present at the same time, then a partial site occupancy is introduced and refined with total occupancy for the two sites fixed to 1.

The structure of $Sr_2Zr(C_2O_4)_4 \cdot 11H_2O$ is built up from a three-dimensional arrangement of strontium and zirconium polyhedra connected by bis-bidentate oxalate units. In each asymmetric unit, there is only one type of strontium atom which is surrounded by nine oxygen atoms (Fig. 5) from two bidentate oxalate units, two monodentate oxalate ligands and three water molecules (the Sr–O distances range from 2.53 to 2.68 Å, Table 5). The SrO_9 polyhedra are edge-shared to form mono-dimensional $^{1}_{\infty}[SrO_4(H_2O)_3]$ chains running down the *c*-axis. The zirconium atom is eight-fold coordinated by four bidentate oxalate ligands (the Zr–O distances range from 2.18 to 2.21 Å) and using the criteria developed by HAIGH [22] previously described, its environment is classified as dodecahedral (16th, 17th, 18th lowest O–Zr–O angles are equal to 94.01°). Two successive strontium polyhedra chains are not directly connected. The zirconium polyhedra are isolated one from another but are linked through bidentate oxalate ligands to the strontium polyhedra chains leading to a three dimensional network. In fact one ZrO_8 dodecahedron is connected to four different chains through four oxalate groups. The resulting structure exhibits square channels running down the *c*-axis (edge dimension section about 6 Å). There are two types of water molecules in this compound, the Ow(1) and O(w2) water molecules belong to the strontium coordination sphere while the two remaining free molecules O(w3) and O(w4) occupy the square channels and present a zeolithic character (Fig. 6).

As in the previous compound, the various distances (average C–O = 1.25 Å and C–C = 1.54 Å) and angles (average O–C–O = 127°(1) and O–C–C = 117°(1)) in the oxalate ligands agree with the previously reported values.

Table 4
Atomic coordinates and equivalent isotropic displacement parameters (Å^2) for $Sr_2Zr(C_2O_4)_4 \cdot 11H_2O$

Atom	Site	Occup	*x*	*y*	*z*	U_{eq}
Sr	16*e*	1	1/4	0.5128(1)	1/2	0.023(1)
Zr	8*a*	1	1/2	3/4	0.08750	0.013(1)
O(1)	32*g*	1	0.1846(2)	0.5622(2)	0.6275(1)	0.028(1)
O(2)	32*g*	1	0.4440(2)	0.6954(2)	0.9741(1)	0.031(1)
O(3)	32*g*	1	0.4084(2)	0.8423(2)	0.9066(1)	0.030(1)
O(4)	32*g*	1	0.3517(2)	0.3932(2)	0.4787(2)	0.057(1)
C(1)	32*g*	1	0.6346(2)	0.8821(2)	0.8902(2)	0.023(1)
C(2)	32*g*	1	0.6123(2)	0.8592(2)	0.9696(2)	0.030(1)
O(w1A)	32*g*	0.72(1)	0.3741(13)	0.5936(9)	0.5483(8)	0.096(5)
O(w1B)	32*g*	0.28	0.4030(20)	0.5570(40)	0.5260(20)	0.096(5)
O(w2A)	32*g*	0.41(1)	0.2610(30)	0.6779(7)	0.5080(20)	0.138(9)
O(w2B)	32*g*	0.09	0.1770(70)	0.6450(50)	0.4643(18)	0.138(9)
O(w3)	8*b*	1	1/2	3/4	0.11250	0.099(5)
O(w4A)	32*g*	0.66(1)	0.7718(14)	0.7602(6)	0.8733(6)	0.091(4)
O(w4B)	32*g*	0.34	0.8230(30)	0.7604(10)	0.8777(7)	0.091(4)

U_{eq} is defined as one third of the trace of the orthogonalized U_{ij} tensor.

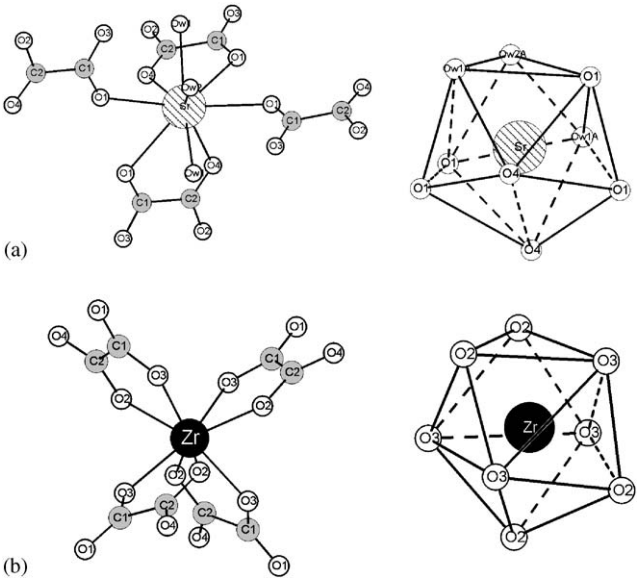

Fig. 5. Coordination spheres for strontium (a) and zirconium (b) atoms in $Sr_2Zr(C_2O_4)_4 \cdot 11H_2O$. The water molecules Ow1 and Ow2 are not split to simplify the representation.

Table 5
Bond lengths (Å) and angles (deg) for $Sr_2Zr(C_2O_4)_4 \cdot 11H_2O$

Within the SrO_9 polyhedra		Within the ZrO_8 polyhedra	
Sr–O(w2B)^{I}	2.53(4)	Zr–O(3)^{II}	2.176(2)
Sr–O(w2B)	2.53(4)	Zr–O(3)^{III}	2.176(2)
Sr–O(w1A)	2.547(18)	Zr–O(3)^{IV}	2.176(2)
Sr–O(w1A)^{I}	2.547(18)	Zr–O(3)	2.176(2)
Sr–O(4) ^{I}	2.563(3)	Zr–O(2)^{IV}	2.206(2)
Sr–O(4)	2.563(3)	Zr–O(2)^{II}	2.206(2)
Sr–O(w1B)	2.614(16)	Zr–O(2)^{III}	2.206(2)
Sr–O(w1B)^{I}	2.614(16)	Zr–O(2)	2.206(2)
Sr–O(w2A)	2.675(12)		
Sr–O(w2A)^{I}	2.675(12)		
Sr–O(1)	2.679(2)		
Sr–O(1)^{I}	2.756(2)		
Sr–O(1)^{II}	2.756(2)		
Sr–O(1)^{III}	2.679(2)		
Within the oxalate groups			
C(1)–O(1)^{VIII}	1.229(4)	O(1)^{VIII}–C(1)–O(3)^{III}	127.1(3)
C(1)–O(3)^{III}	1.272(4)	O(4)^{IX}–C(2)–O(2)^{IV}	126.5(3)
C(1)–C(2)	1.539(5)	O(4)^{IX}–C(2)–C(1)	120.2(3)
C(2)–O(4)^{IX}	1.236(4)	O(2)^{IV}–C(2)–C(1)	113.3(3)
C(2)–O(2)^{IV}	1.267(4)	O(1)^{VIII}–C(1)–C(2)	120.4(3)
		O(3)^{III}–C(1)–C(2)	112.5(3)

Symmetry transformations used to generate equivalent atoms: I, $-x+1/2$, y, $-z+1$; II, $-y+5/4$, $x+1/4$, $-z+7/4$; III, $y-1/4$, $-x+5/4$, $-z+7/4$; IV, $-x+1$, $-y+3/2$, $z+0$; V, $y-3/4$, $-x+5/4$, $z-1/4$; VI, $y-1/4$, $-x+3/4$, $z+1/4$; VII, $-x+1$, $y-1/2$, z; VIII, $-y+5/4$, $x+3/4$, $z+1/4$; IX, $-x+1$, $y+1/2$, $-z+3/2$.

3.2.2. Thermal decomposition

The decomposition of the strontium zirconium oxalate have been found to proceed through three major steps (i) a three stage dehydration, (ii) the oxalate

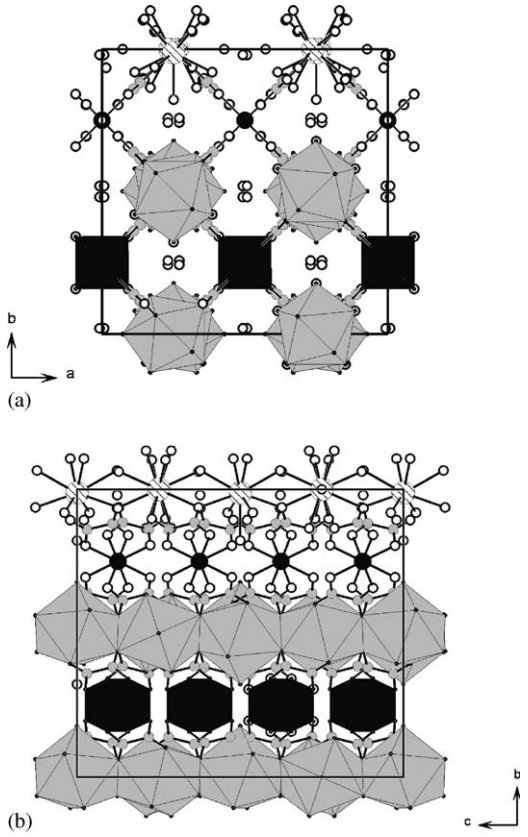

Fig. 6. Views of the structure of $Sr_2Zr(C_2O_4)_4 \cdot 11H_2O$: (a) projection of a complete cell down the *c*-axis showing the connection of the $^1_\infty[SrO_4(H_2O)_3]$ chains by ZrO_8 polyhedra through oxalate ions, (b) projection down the *a*-axis showing the edge sharing of SrO_9 polyhedra to form one-dimensional chains running down the *c*-axis. Large hatching circle, Sr; medium black circle, Zr; small light-gray circle, C; small white circle, O.

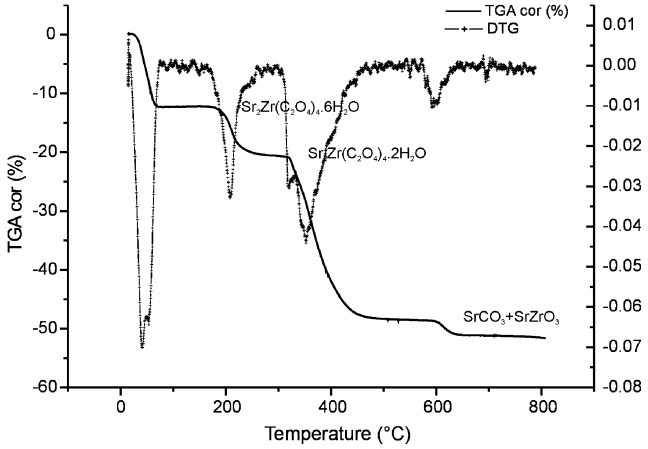

Fig. 7. TG and DTG curves for $Sr_2Zr(C_2O_4)_4 \cdot 11H_2O$ under flowing air ($1\,^\circ C\,min^{-1}$) with identified crystalline compounds. DTG curve is the derivative of the TG curve.

decomposition and (iii) the release of carbon monoxide and carbon.

From the TG measurements, the water content (11.5 water molecules) and the chemical formula ($Sr_2Zr(C_2O_4)_4 \cdot 11.5H_2O$) have been deduced (Fig. 7). The dehydration of $Sr_2Zr(C_2O_4)_4 \cdot 11.5H_2O$ takes place between room temperature and 300 °C in three stages. This number of water molecules is a little higher than the number found by crystal structure determination, it can be explained by absorption of some water on the powder surface. The observed weight losses for the first and the second dehydration steps are 12.1% and 8.9%, respectively against the calculated values 12.0% and 8.7% for 5.5 and 4 water molecules per mole of strontium zirconium oxalate hydrate. During the first dehydration step, all the zeolitic water molecules lying in the tunnels are eliminated, whereas the second stage corresponds to the release of four water molecules of the strontium coordination sphere. The intermediate oxalate compound $Sr_2Zr(C_2O_4)_4 \cdot 6H_2O$ is stable between 70 and 180 °C and well crystallized. The comparison between the HTXRD diagrams at room temperature and at 150 °C (Fig. 8), shows that the crystallographic structures of $Sr_2Zr(C_2O_4)_4 \cdot 11.5H_2O$ and $Sr_2Zr(C_2O_4)_4 \cdot 6H_2O$ are different but present some similarities as attested by the position of the main reflections. Actually the powder pattern at 150 °C can be indexed with a tetragonal unit cell with parameters $a = 15.973(2)$ Å and $c = 8.715(1)$ Å, systematic absences indicate $P4_2/ncm$ and $P4_2/nnm$ as possible space groups. The third stage of the dehydration is combined in TG analysis with the oxalate decomposition. From the DTG curve (Fig. 7), it is evident that before the dehydration is complete, the oxalate decomposition starts. This stage occurs between 300 and 500 °C and involves a complex set of reactions which leads to the formation of a black mixture of strontium carbonate, strontium zirconium oxide, carbon and perhaps an amorphous oxycarbonate. Then, it is not possible to determine the precise composition of this residue by comparison of the experimental weight loss with the calculated value. Indeed, the HTXRD diagram at 600 °C could confirm only the presence of crystallized $SrCO_3$ and $SrZrO_3$. The presence of carbon in the residue of the oxalate decomposition has already been mentioned by Reddy et al. [10] in their work on the thermal decomposition of strontium zirconyl oxalate hexahydrate. This carbon is produced during the carbon monoxide disproportionation.

The last stage occurs between 600 and 650 °C and corresponds to the release of carbon monoxide as a result of the oxidation of carbon and leads to a white powder, well crystallized, which contains: $SrCO_3 + SrZrO_3$ (weight loss 52%, expected value 54.6%). This relatively important difference between the experimental and the theoretical value of the weigh loss could be explained by the presence of another compound in the final mixture, but the HTXRD diagrams and the X-ray analysis of the TG residue at 800 °C, allow only the identification of crystallized $SrCO_3$ and $SrZrO_3$.

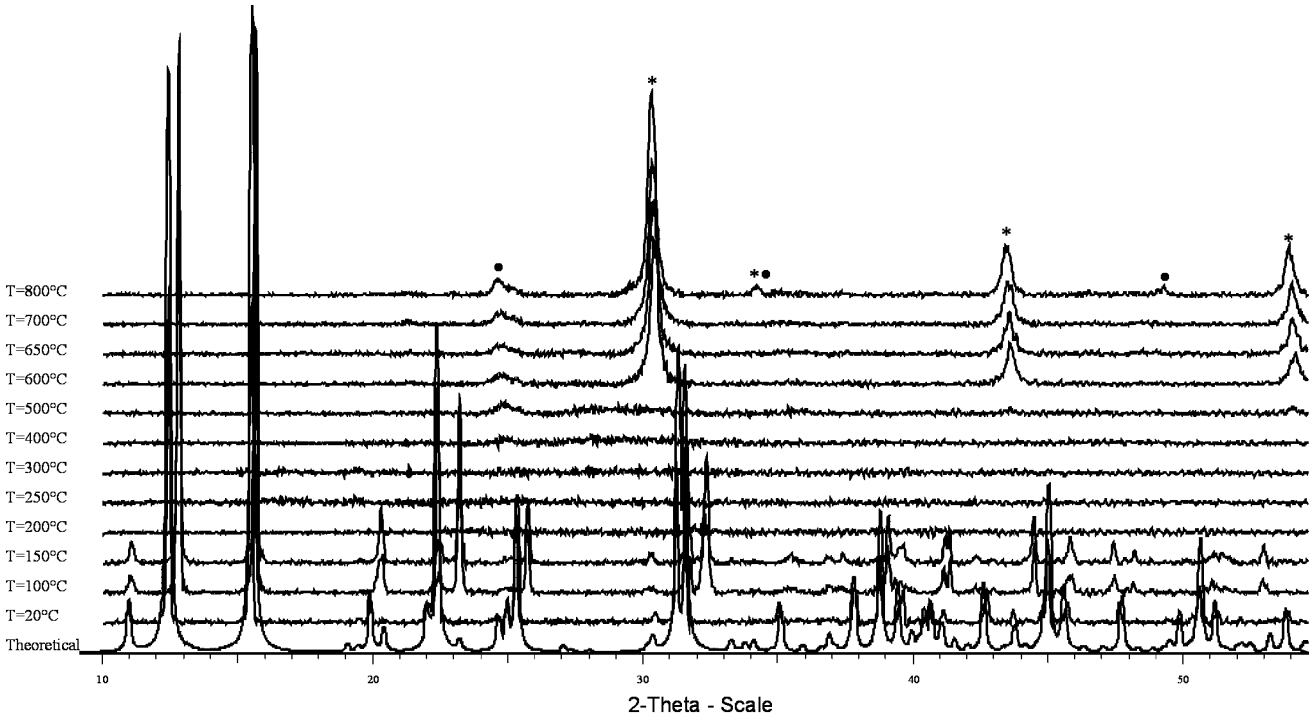

Fig. 8. HTXRD plot for $Sr_2Zr(C_2O_4)_4 \cdot 11H_2O$ under flowing air; ●, diffraction lines from $SrCO_3$; ∗, diffraction lines from $SrZrO_3$. The X-ray diagram noted "theoretical" is calculated from the single-crystal data by the software POWDERCELL.

3.3. $Ca_2Zr(C_2O_4)_4 \cdot 5H_2O$

3.3.1. Structure description

The structure determination was not immediate. Contrary to the strontium compound which gave geometrically perfect crystals, the crystals had slightly irregular surfaces and were often visibly twinned. When a "good" small (<100 μm) sample was examined, it gave a tetragonal cell ($a = 11.246(1)$, $c = 8.412(2)$ Å). The best solution was obtained in space group $I\bar{4}$ but it was not satisfactory. With a bigger crystal, the presence of some weak reflections led to a larger cell ($a\sqrt{2} = 15.888(2)$ Å, $b\sqrt{2} = 15.888(2)$ Å, $c = 8.418(2)$ Å). However, no space group in this tetragonal cell could get a satisfactory solution. Finally, consideration of an orthorhombic cell with a twinning gave a solution which was acceptable both in crystallographic and chemical terms. The crystal structure was solved in space groups *Pna*21 with a cell $a = 8.418(2)$ Å, $b = 15.888(2)$ Å, $c = 15.888(2)$ Å, twinning along bc diagonal (volume ratio 0.477) with unit weighing scheme (to better take into account the weak reflections) and some constraints on C–C distances to prevent oxalate deformations (Table 6).

The double oxalate $Ca_2Zr(C_2O_4)_4 \cdot 5H_2O$ exhibits a three-dimensional arrangement of calcium and zirconium polyhedra linked through oxalate bridges. The zirconium atom is eight-fold coordinated by oxygen atoms (distances Zr–O range from 2.14 to 2.24 Å, Table 7) from four bidentate oxalate ligands. From the comparison of the 16th, 17th, 18th lowest O–Zr–O angles (91.3°, 92.1°, 103.2°, respectively), the ZrO_8 polyhedra can be described as biccaped trigonal prisms (Fig. 9c) according to the HAIGH criteria [22]. In this structure, there are two independent calcium atoms which are both eight-fold coordinated and have the same type of environment built from two bidentate oxalate ligands, two monodentate oxalate groups and two water molecules. The eight oxygen atoms surrounding atom Ca(1) are located between 2.38 and 2.58 Å and form a square antiprism distorted towards biccaped trigonal prism (16th, 17th, 18th lowest O–Ca(1)–O angles are 89.2°, 96.7°, 107.4°, Fig. 9a). The $Ca(2)O_8$ polyhedron can also be classified as square antiprism distorted towards biccaped trigonal prism (16th, 17th, 18th O–Ca(2)–O angles are 89.8°, 96.1°, 106.3°, Fig. 9b) and distances Ca(2)–O range from 2.37 to 2.58 Å). The $Ca(1)O_8$ polyhedra are connected by sharing O(2)–O(4) edges to form $^1_\infty[Ca(1)O_4(H_2O)_2]$ chains running down [100]. Similarly $^1_\infty[Ca(2)O_4(H_2O)_2]$ chains running down [100] result from O(1)–O(3) edge-shared $Ca(2)O_8$ polyhedra. The zirconium polyhedra are localized between the different chains of calcium polyhedra and each zirconium polyhedron is connected to four calcium polyhedra through bis-bidentate oxalate bridges. The resulting three-dimensional arrangement exhibits square tunnels along [100] in which lie the zeolitic water molecule O(5w) (Fig. 10). In fact, apart from some

Table 6
Atomic coordinates ($\times 10^4$) and equivalent isotropic displacement parameters (Å^2) for $Ca_2Zr(C_2O_4)_4 \cdot 5H_2O$

Atom	x	y	z	U_{eq}
Zr	0.7487(2)	0.49976(8)	0.0369	0.018(1)
Ca(1)	0.9978(4)	0.24069(16)	0.6194(2)	0.024(1)
Ca(2)	0.9974(3)	0.73964(15)	0.6184(2)	0.020(1)
O(1)	0.7446(9)	0.6918(6)	0.5505(6)	0.017(2)
O(2)	0.7476(10)	0.3055(6)	0.5518(6)	0.019(2)
O(3)	0.7497(10)	0.8166(6)	0.6731(6)	0.019(2)
O(4)	0.7468(11)	0.1833(6)	0.6746(6)	0.021(2)
O(5)	0.8206(9)	0.3980(4)	0.2851(5)	0.016(2)
O(6)	0.5312(8)	0.5604(4)	0.4219(5)	0.012(1)
O(7)	0.8224(12)	0.5918(6)	0.4622(6)	0.034(2)
O(8)	1.0632(11)	0.3601(6)	0.5271(6)	0.027(2)
O(9)	1.0591(12)	0.8419(6)	0.7251(6)	0.029(2)
O(10)	0.9361(11)	0.8566(6)	0.5251(6)	0.025(2)
O(11)	0.6779(10)	0.4118(5)	0.4669(6)	0.025(2)
O(12)	0.9637(13)	0.4370(6)	0.4202(7)	0.036(2)
O(13)	0.9372(11)	0.3438(5)	0.7244(6)	0.024(2)
O(14)	0.6794(13)	0.6005(6)	0.2818(7)	0.036(2)
O(15)	0.9659(10)	0.5519(5)	0.3059(5)	0.019(2)
O(16)	0.5378(11)	0.4504(6)	0.3036(6)	0.033(2)
C(1)	0.9475(14)	0.3855(7)	0.4795(8)	0.025(3)
C(2)	1.0452(16)	0.3838(8)	0.7623(9)	0.030(3)
C(3)	0.5428(16)	0.6135(7)	0.4819(8)	0.022(2)
C(4)	0.9498(14)	0.8910(7)	0.7548(7)	0.018(2)
C(5)	0.7866(14)	0.6326(7)	0.2340(8)	0.021(2)
C(6)	0.7714(11)	0.3576(6)	0.4998(6)	0.08(2)
C(7)	0.7223(16)	0.6372(7)	0.4982(8)	0.021(3)
C(8)	0.7233(19)	0.3695(8)	0.2325(9)	0.034(3)
O(w1)	0.8900(14)	0.6483(8)	0.7240(8)	0.050(3)
O(w2)	0.1046(16)	0.1522(8)	0.7265(9)	0.058(3)
O(w3)	0.8962(11)	0.1312(6)	0.5327(7)	0.030(2)
O(w4)	1.1029(12)	0.6314(6)	0.5321(7)	0.033(2)
O(w5)	0.0262(4)	0.4987(15)	0.6195(13)	0.147(7)

U_{eq} is defined as one third of the trace of the orthogonalized U_{ij} tensor.

Table 7
Bond lengths (Å) and angles (deg) for $Ca_2Zr(C_2O_4)_4 \cdot 5H_2O$

Within the $Ca(1)O_8$ polyhedra		Within the ZrO_8 polyhedra	
Ca(1)–O(2)	2.579(10)	Zr–O(5)	2.180(7)
Ca(1)–O(2)^{I}	2.472(10)	Zr–O(6)	2.233(7)
Ca(1)–O(4)	2.463(10)	Zr–O(7)	2.172(10)
Ca(1)–O(4)^{I}	2.573(10)	Zr–O(11)	2.174(9)
Ca(1)–O(8)	2.460(10)	Zr–O(12)	2.221(11)
Ca(1)–O(13)	2.393(10)	Zr–O(14)	2.196(10)
Ca(1)–O(w3)	2.378(10)	Zr–O(15)	2.243(8)
Ca(1)–O(w2)	2.384(14)	Zr–O(16)	2.201(10)
Within the $Ca(2)O_8$ polyhedra			
Ca(2)–O(1)	2.504(9)		
Ca(2)–O(1)^{II}	2.585(9)		
Ca(2)–O(3)	2.569(9)		
Ca(2)–O(3)^{II}	2.462(9)		
Ca(2)–O(9)	2.405(10)		
Ca(2)–O(10)	2.433(10)		
Ca(2)–O(w4)	2.373(10)		
Ca(2)–O(w1)	2.395(13)		
Within the oxalate groups			
C(1)–O(8)	1.297(15)	O(8)–C(1)–O(12)	124.0(11)
C(1)–O(12)	1.255(16)	O(8)–C(1)–C(6)	119.8(10)
C(1)–C(6)	1.581(15)	O(12)–C(1)–C(6)	116.0(10)
C(6)–O(2)	1.186(13)	O(2)–C(6)–O(11)	130.6(10)
C(6)–O(11)	1.279(12)	O(2)–C(6)–C(1)	119.8(9)
		O(11)–C(6)–C(1)	107.7(8)
C(2)–O(13)	1.263(17)	O(13)–C(2)–O(15)^{IV}	128.9(13)
C(2)–O(15)^{IV}	1.237(16)	O(13)–C(2)–C(5)^{IV}	116.5(12)
C(2)–C(5)^{IV}	1.508(18)	O(15)^{IV}–C(2)–C(5)^{IV}	112.4(11)
C(5)–O(4)^{VII}	1.273(16)	O(4)^{VII}–C(5)–O(14)	122.3(11)
C(5)–O(14)	1.284(16)	O(4)^{VII}–C(5)–C(2)^{VIII}	122.6(11)
		O(14)–C(5)–C(2)^{VIII}	114.5(11)
C(3)–O(6)	1.278(14)	O(6)–C(3)–O(10)^{V}	128.1(12)
C(3)–O(10)^{V}	1.226(16)	O(6)–C(3)–C(7)	110.7(10)
C(3)–C(7)	1.578(19)	O(10)^{V}–C(3)–C(7)	121.2(11)
C(7)–O(1)	1.216(15)	O(1)–C(7)–O(7)	128.4(12)
C(7)–O(7)	1.248(16)	O(1)–C(7)–C(3)	115.5(11)
		O(7)–C(7)–C(3)	115.7(10)
C(4)–O(9)	1.295(15)	O(9)–C(4)–O(16)^{VI}	129.2(12)
C(4)–O(16)^{VI}	1.227(15)	O(9)–C(4)–C(8)^{VI}	117.2(10)
C(8)–C(4)^{III}	1.538(20)	O(16)^{VI}–C(4)–C(8)^{VI}	113.4(11)
C(8)–O(3)^{III}	1.284(17)	O(3)^{III}–C(8)–O(5)	127.6(13)
C(8)–O(5)	1.255(16)	O(3)^{III}–C(8)–C(4)^{III}	118.8(12)
		O(5)–C(8)–C(4)^{III}	112.6(11)

Symmetry transformations used to generate equivalent atoms: I, $1+x$, $1-y$, $1/2+z$; II, $1+x$, $2-y$, $1/2+z$; III, $3/2-x$, $-1/2+y$, $-1/2+z$; IV, $2-x$, $1-y$, $1/2+z$; V, x, $2-y$, $1/2+z$; VI, $3/2-x$, $1/2+y$, $1/2+z$; VII, $3/2-x$, $1/2+y$, $-1/2+z$; VIII, $2-x$, $1-y$, $-1/2+z$.

slight distortions, the structure is close to the arrangement found in tetragonal $Sr_2Zr(C_2O_4)_4 \cdot 11H_2O$. The zeolitic character of O(5w) has been proved by collecting data on the same crystal, at 100 °C. The structure remains identical, apart the occupancy of the tunnels which fall down to zero.

3.3.2. Thermal decomposition

The thermal decomposition of $Ca_2Zr(C_2O_4)_4 \cdot 5H_2O$ seems to be more complicated to explain than those of $Ba_2Zr(C_2O_4)_4 \cdot 7H_2O$ and $Sr_2Zr(C_2O_4)_4 \cdot 11H_2O$. Indeed, on the TG curve (Fig. 11), the different steps of the dehydration and decomposition overlap and the residues are difficult to identify. However, as for the two precedent compounds, three stages can be distinguished (i) the dehydration in two steps, (ii) the oxalate decomposition and (iii) the release of CO and C. The first step of dehydration, between room temperature and 60 °C, leads to $Ca_2Zr(C_2O_4)_4 \cdot 4H_2O$ (weigh loss 2.5% against calculated value 2.96%) which is stable until 200 °C. The comparison between the HTXRD diagrams at room temperature and at 200 °C shows some similarities but also some small differences. It seems that it is between room temperature and 100 °C that the major evolution take place: for example a small shift of the crystallographic peaks and sometimes a splitting of some reflections (for example around $2\theta = 33°$) are observed for the high 2θ values ($2\theta > 30°$) (Fig. 12). This implies that $Ca_2Zr(C_2O_4)_4 \cdot 5H_2O$ and $Ca_2Zr(C_2O_4)_4 \cdot 4H_2O$ must have close crystallographic

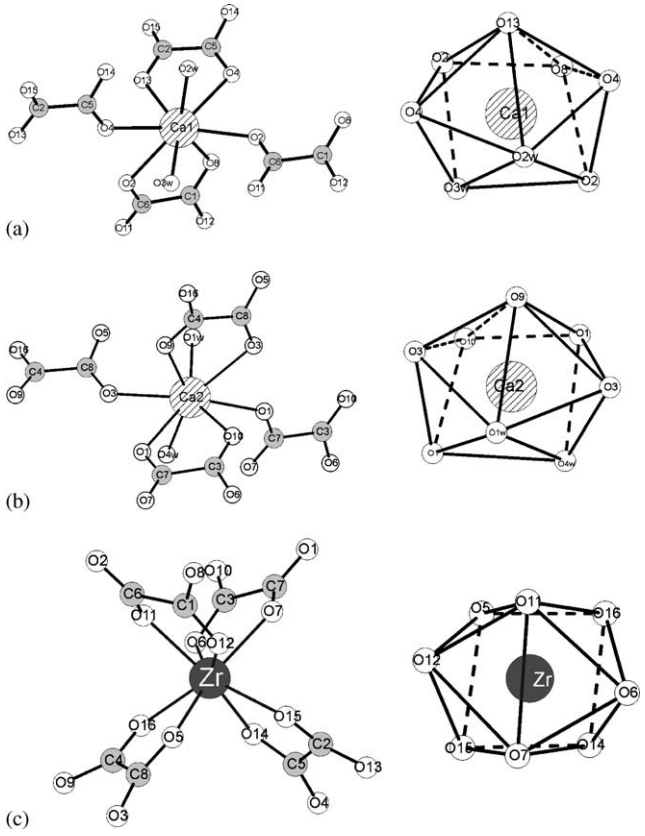

Fig. 9. Coordination spheres for (a) Ca(1), (b) Ca(2) and (c) Zr in $Ca_2Zr(C_2O_4)_4 \cdot 5H_2O$.

structure which is confirmed by single X-ray diffraction. Indeed, the structures determined at room temperature and at 100 °C differ only by the presence or not of one zeolitic water molecule in the square tunnels. The loss of this water molecule leads to small evolutions of the cell without affecting the crystal framework. Beyond 200 °C, starts the second dehydration stage which leads to the anhydrous oxalate compound. The observed weigh loss (15.0%) agrees well with the expected value (14.6%). This oxalate is not stable and its decomposition certainly overlaps its formation. Moreover it is amorphous and consequently very difficult to characterize. The oxalate decomposition takes place between 300 and 680 °C and no resulting product can be isolated because the release of CO and C, at nearly 680 °C overlaps with the end of this decomposition. The TG residue at 600 °C is grayish so the carbon content must be low. The HTXRD diagrams at 500 °C allows the identification of calcium carbonate formation. The final product is a white powder of supposed composition : $\frac{3}{4}CaCO_3 + \frac{1}{2}CaZrO_3 + \frac{1}{4}CaO$ (weight loss 54.1% against calculated value 56.1%). At 800 °C, CaO and $CaZrO_3$ are identified by HTXRD, $CaCO_3$ is not visible anymore on the X-ray diagram at this temperature but it must be still in the residue because the calcite decomposes only beyond 898 °C. Other intermediate carbonates have

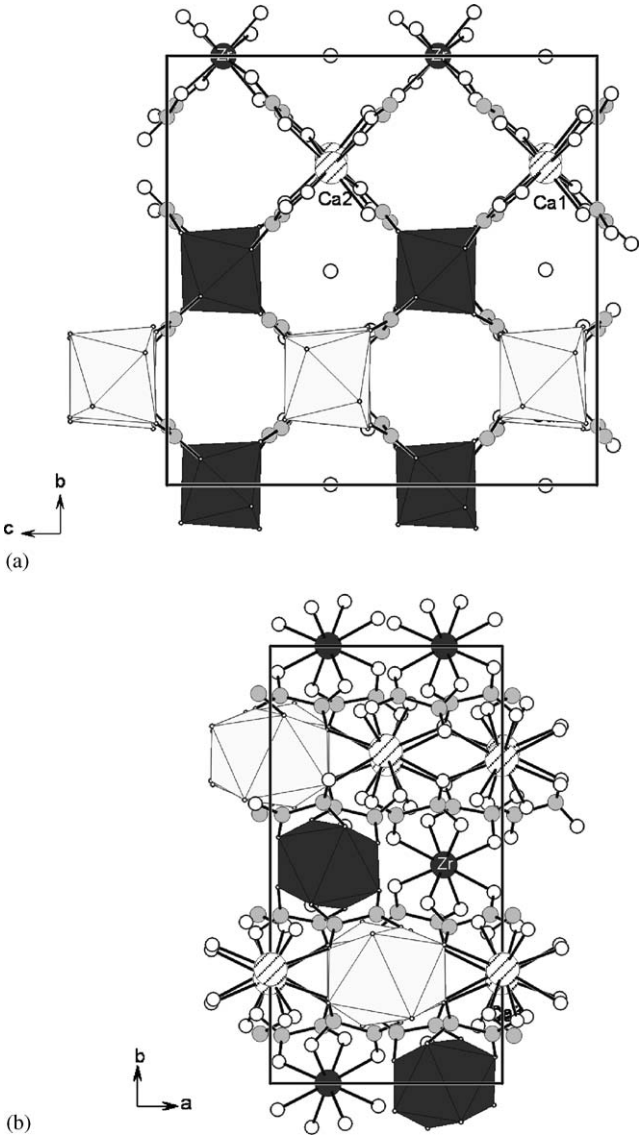

Fig. 10. Projections of the structure of $Ca_2Zr(C_2O_4)_4 \cdot 5H_2O$ down the *a*-axis (a) and down the *c* -axis (b) showing the connection of $^1_\infty[CaO_4(H_2O)_2]$ chains by ZrO_8 polyhedra through the oxalate moieties creating large tunnels running down the *a*-axis, which are occupied by zeolitic water molecules. Large hatching circle, Ca(1) and Ca(2); medium black circle, Zr; small light-gray circle, C; small white circle, O.

already been mentioned ($Ca_2Zr_2O_4(CO_3)_2$ [12,15], $Ca_2Zr_2O_{4+x}(CO_3)_{2-x}$, and $Ca_2Zr_2O_{4+x}(CO_3)_{2-x}(CO_2)_x$ [11]) but none of these compounds could be clearly identified during the thermal decomposition of $Ca_2Zr(C_2O_4)_4 \cdot 5H_2O$.

4. Conclusion

The present study leads to the classification of $M_2Zr(C_2O_4)_4 \cdot nH_2O$ compounds in two types of crystal structures both exhibiting a three-dimensional

framework architecture composed of a linked network of $^1_\infty[MO_4(H_2O)_3]$ chains and ZrO_8 polyhedra via coordinating $C_2O_4^{2-}$ anions. In both crystal structure types, of the three oxalate units that link with the M atom, two have the normal bis-bidentate connectivity and the remaining oxalate is shared between two neighboring M atoms via a three coordinated oxygen ($\mu-3$ oxygen) leading to the formation of zig-zag chains of edge-shared MO_{6+x} polyhedra. The chains are linked to ZrO_8 polyhedra via oxalate ions that act as bis-bidentate. In both cases, the relatively open nature of the Zr^{4+}/M^{2+}/oxalate framework allows the coordination of the M^{2+} ions by water molecules. For the first structure type, which can be found for the smallest M cations (Ca, Sr and Cd), the $^1_\infty[MO_4(H_2O)_3]$ chains are all parallel. ZrO_8 polyhedra connect four of these parallel chains in a way that square channels are formed which can accommodate zeolitic water molecules. The symmetry is tetragonal or pseudo-tetragonal with the c-axis corresponding to the chains direction. The ZrO_8 polyhedron is a dodecahedron. The mixed oxalates with the largest M cations (Ba and Pb) adopt another structure, with all chains arranged in parallel in planes perpendicular to the b-axis of the monoclinic unit cell. Between two successive planes the chains are rotated of about 60° and connected by ZrO_8 polyhedra through oxalate ions. The ZrO_8 polyhedron is described as a square antiprism.

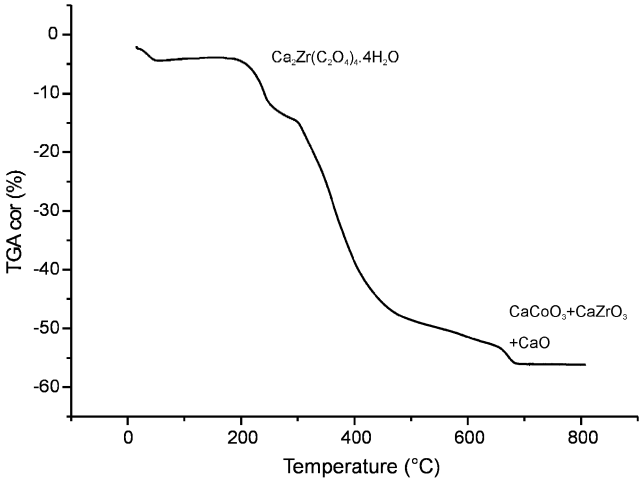

Fig. 11. TG curve of $Ca_2Zr(C_2O_4)_4\cdot 5H_2O$ under flowing air ($1\,^\circ C\,min^{-1}$) with identified crystalline compounds.

The products resulting from the decomposition of $M_2Zr(C_2O_4)_4\cdot nH_2O$ compounds at 800 °C under flowing air are mixtures of $MZrO_3$ perovskites accompanied by alkaline earth carbonate (for $M=$Ba or Sr) or oxide (for $M=$Ca) and of metallic lead for $M=$Pb (2), for $M=$Cd a mixture of CdO and cubic "ZrO_2" was obtained [6].

The preparation and thermal decomposition of zirconyl oxalates of Sr, Ca and Ba have been reported in the

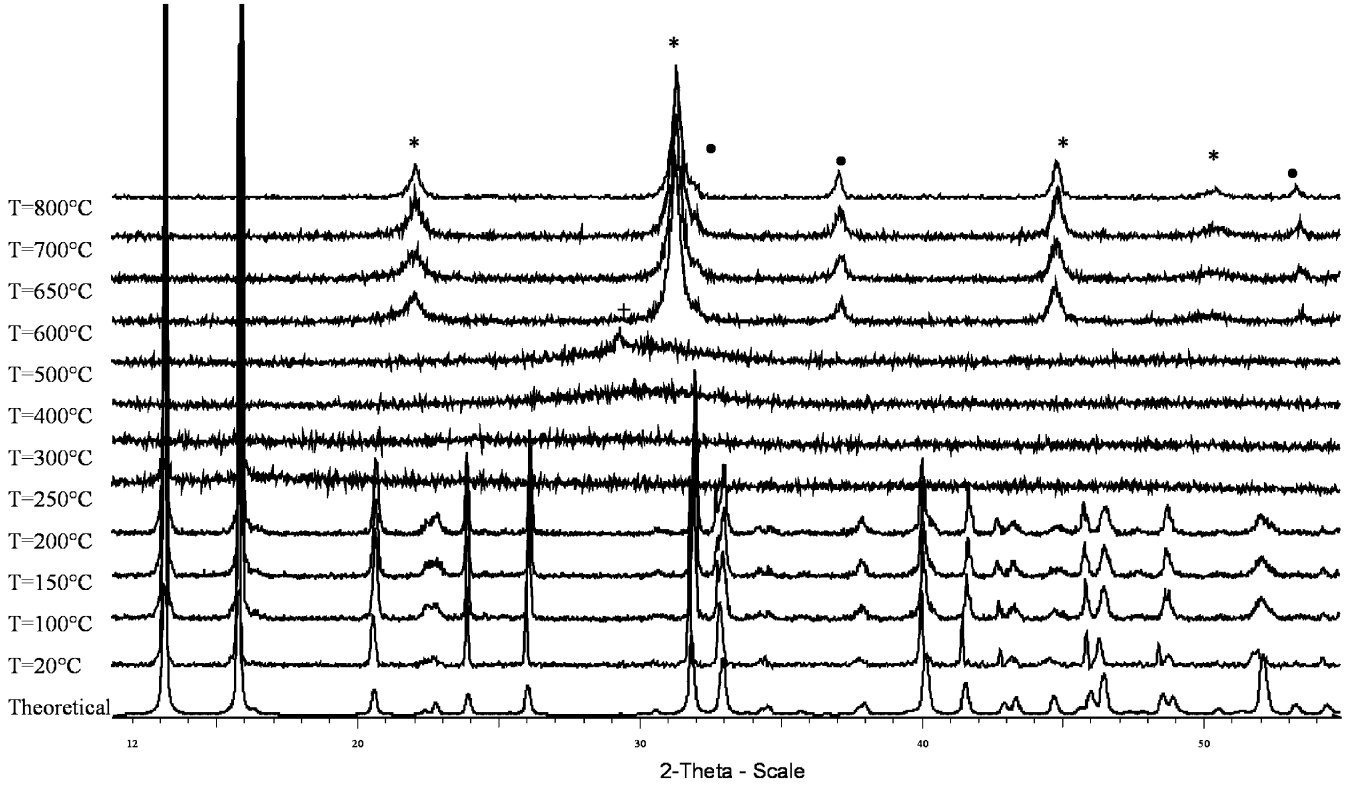

Fig. 12. HTXRD plot for TG curve for $Ca_2Zr(C_2O_4)_4\cdot 5H_2O$; ●, diffraction lines from CaO; ∗, diffraction lines from $CaZrO_3$; + diffraction line from $CaCO_3$. The X-ray diagram noted "theoretical" is calculated from the single-crystal data by the software POWDERCELL.

literature [9–16]. Unfortunately, zirconyl oxalates $MZrO(C_2O_4)_2 \cdot nH_2O$ have not been structurally characterized and their formation is doubtful. The decomposition of $CaZr(C_2O_4)_3 \cdot H_2O$ to $CaZrO_3$ has also been reported but the starting oxalate was not better characterized [17]. In fact the majority of the X-ray patterns given by the different authors match well to the theoritical ones calculated from the single-crystal structure determination results which are identical to the patterns of the reported $M_2Zr(C_2O_4)_4 \cdot nH_2O$ compounds.

Acknowledgments

Financial support from COGEMA (France) is gratefully acknowledged.

References

[1] W.S. Clabaugh, E.M. Swiggard, R. Gilchrist, J. Res. Natl. Bur. Stand. 56 (1957) 289.
[2] C. Boudaren, J.P. Auffredic, M. Louër, D. Louër, Chem. Mater. 12 (2000) 2324.
[3] E. Jeanneau, N. Audrebrand, D. Louër, Chem. Mater. 14 (2002) 1187.
[4] E. Jeanneau, N. Audrebrand, M. Le Floch, B. Bureau, D. Louër, J. Solid State Chem. 170 (2003) 330.
[5] G.L. Glen, J.V. Silverton, J.L. Hoard, Inorg. Chem. 2 (1963) 250.
[6] E. Jeanneau, N. Audrebrand, J.P. Auffredic, D. Louër, J. Mater. Chem. 11 (2001) 2545.
[7] E. Jeanneau, N. Audrebrand, D. Louër, J. Mater. Chem. 12 (2002) 2383.
[8] J.L. Shi, Z.X. Lin, Solid State Ionics 32/33 (1989) 544.
[9] V.B. Reddy, P.N. Mehrotra, Thermochim. Acta 31 (1979) 31.
[10] V.B. Reddy, P.N. Mehrotra, Thermochim. Acta 31 (1979) 349.
[11] V.B. Reddy, P.N. Mehrotra, J. Inorg. Nucl. Chem. 43 (1981) 1078.
[12] T. Gangadevi, M. Subra Rao, T.R. Narayanan Kutty, Indian J. Chem. 19A (1980) 309.
[13] T. Gangadevi, M. Subra Rao, T.R. Narayanan Kutty, J. Therm. Anal. 19 (1979) 321.
[14] T. Gangadevi, K. Muraleedharan, M.P. Kannan, Thermochim. Acta 144 (1989) 109.
[15] T. Gangadevi, K. Muraleedharan, M.P. Kannan, Thermochim. Acta 146 (1989) 225.
[16] Y. Saikali, M. Roubin, B. Durand, Ann. Chim. Fr. 17 (1992) 123.
[17] M.J. Saavedra, C. Parada, M.O. Figueiredo, A. Correa Dos Santos, Solid State Ionics 63–65 (1993) 213.
[18] H.K. Henisch, Crystals in Gels and Liesegangs rings, The Pennsylvania State University Press, University Park, London, 1988.
[19] Bruker Analytical X-ray system, "SAINT+, Version 6.22", Madison, USA, 2001.
[20] V. Petricek, M. Dusek, The Crystallographic Computing System JANA2000, Praha, Czech Republic, 2002.
[21] G.M. Scheldrick, SADABS, Bruker-Siemens Area Detector Absorption and Other Correction, Version 2.03, Goetingen, Germany, 2001.
[22] C.W. Haigh, Polyhedron 14 (20–21) (1995) 2871.
[23] T. Hahn, Z. Anorg. Allg. Chem. 109 (1957) 438.